



**University of  
Zurich**<sup>UZH</sup>

**Zurich Open Repository and  
Archive**

University of Zurich  
University Library  
Strickhofstrasse 39  
CH-8057 Zurich  
[www.zora.uzh.ch](http://www.zora.uzh.ch)

---

Year: 2021

---

## **Analytic series expansion of the overlap reduction function for gravitational wave search with pulsar timing arrays**

Boëtier, Adrian ; Tiwari, Shubhanshu ; Jetzer, Philippe

**Abstract:** In our previous paper A. Boëtier et al. [Phys. Rev. D 102, 064051 (2020)], we derived a generic expression for the pulse redshift, the main observable for the Pulsar Timing Array (PTA) experiment for detection of gravitational waves for all possible polarizations induced by modifications of general relativity. In this work, we provide a generic expression of the overlap reduction function for PTA without using the short wavelength approximation for tensorial polarization. We find that when the overlap reduction function does not have the exponential terms, which is the case when using short wavelength approximation, it leads to discontinuities and poles. In this work, we provide a series expansion to calculate the integral exactly and investigate the behavior of the series for short wavelength values via numerical evaluation of the analytical series. We find a disagreement for the limit of colocated pulsars with the Hellings and Downs curve. Otherwise, our formalism agrees with the Hellings and Downs curve for a broad range of pulsars.

DOI: <https://doi.org/10.1103/physrevd.103.064044>

Posted at the Zurich Open Repository and Archive, University of Zurich

ZORA URL: <https://doi.org/10.5167/uzh-202931>

Journal Article

Published Version

Originally published at:

Boëtier, Adrian; Tiwari, Shubhanshu; Jetzer, Philippe (2021). Analytic series expansion of the overlap reduction function for gravitational wave search with pulsar timing arrays. Physical review D, 103:064044. DOI: <https://doi.org/10.1103/physrevd.103.064044>

# Analytic series expansion of the overlap reduction function for gravitational wave search with pulsar timing arrays

Adrian Boëtier<sup>\*,†</sup>, Shubhanshu Tiwari<sup>‡</sup> and Philippe Jetzer<sup>‡</sup>

*Physik-Institut, Universität Zürich, Winterthurerstrasse 190, 8057 Zürich, Switzerland*



(Received 23 September 2020; accepted 22 February 2021; published 22 March 2021)

In our previous paper A. Boëtier *et al.* [*Phys. Rev. D* **102**, 064051 (2020)], we derived a generic expression for the pulse redshift, the main observable for the Pulsar Timing Array (PTA) experiment for detection of gravitational waves for all possible polarizations induced by modifications of general relativity. In this work, we provide a generic expression of the overlap reduction function for PTA without using the short wavelength approximation for tensorial polarization. We find that when the overlap reduction function does not have the exponential terms, which is the case when using short wavelength approximation, it leads to discontinuities and poles. In this work, we provide a series expansion to calculate the integral exactly and investigate the behavior of the series for short wavelength values via numerical evaluation of the analytical series. We find a disagreement for the limit of colocated pulsars with the Hellings and Downs curve. Otherwise, our formalism agrees with the Hellings and Downs curve for a broad range of pulsars.

DOI: [10.1103/PhysRevD.103.064044](https://doi.org/10.1103/PhysRevD.103.064044)

## I. INTRODUCTION

In our previous paper, we calculated the redshift of Pulsar Timing Array (PTA) pulses under the influence of gravitational waves with all six possible polarizations in modified general relativity (GR) [1]. We use our previous result up to first order in the strain  $h$  and zeroth order in gravitational wave frequency times pulsar period  $\omega T_a$  to calculate the cross-correlated signal for the gravitational wave background (GWB). We collect all direction integrals over geometric terms in the overlap reduction function. This includes the interference terms which we exclude from the pattern functions as we argued in our previous work; thus, we arrive at the same integral as the present literature [2] currently in use with the search of gravitational waves with PTA [3–5]. When calculating the integral, however, we do not rely on the short wavelength approximation. In Appendix B, we *prove* that the short wavelength can be safely used under the condition (B8). Since this condition is not met by the overlap reduction function due to the poles in the integrand, we cannot be sure that the approximation can be made. Instead, we express the integrand as a Laurent series and determine the integral via residue theorem. We find that our series agrees with the Hellings and Downs (H&D) curve in the entire parameter space except for a neighborhood around  $\phi = 0$  and  $L = L'$ , i.e., colocated pulsars like PSR J0737-3039 [6], which should both be

visible again in 2035. This puts the approximation on solid mathematical footing. Our formalism is also applicable to other polarizations and leads to a generically valid expression for any pulsar found and still holds for much higher frequencies and shorter distances.

A gravitational wave background would introduce a characteristic redshift imprint on a collection of pulsars, which depends on their location on the sky and distance from Earth. Knowing these quantities would allow us to recognize (identify) such a signal (a signal with these properties) as a GWB. This can be achieved via matched filtering, where one uses the expected imprint as a filter function to extract a signal from the noisy data that match the filter. For this to work, the expected signal must be predicted correctly up to an error of roughly  $\pm 3\%$  [7].

The geometric part of the expected response of the cross-correlated signal of two pulsars is called the overlap reduction function and is an essential part of the filter function. It is an integral over the unit sphere, and since the integrand contains exponential terms which make an integration difficult, one usually refers to the *short* wavelength approximation to drop out these terms. This way, one arrives at the Hellings and Downs curve [8]. We would like to point out that this function is *a priori* not defined at 0 but can be continuously extended.

By plotting the pattern functions, which are usually used, we spotted that there always is a discontinuity for  $+$ ,  $\times$ , and a pole for  $x$ ,  $y$ , and  $l$  polarization for each pulsar in the integration domain. This always occurs when the source lies directly behind the pulsar. This ill-defined point is forced to zero by the exponential terms. So, if the

\*boitier@physik.uzh.ch

†stiwari@physik.uzh.ch

‡jetzer@physik.uzh.ch

exponential terms are neglected due to short wavelength approximation, then the integrand is ill defined on its integration domain. Therefore, we calculate the integral without this approximation. Since it is not obvious to us how one could compute the limit of our result, we investigate its behavior for long wavelengths by numerically evaluating the resulting series for increasing values of  $L\omega$ .

We find that, except one special case, the series converges to the H&D curve as expected. However, for the special case where the two pulsar distances are almost the same and they are very close to each other on the sky (best example: double pulsar system), the series tends to the value 2 instead of 1.

We derive the signal-to-noise ratio (SNR) for a GWB measurement using PTA's in Sec. II and extract the expression for the overlap reduction function for the tensor mode from this calculation. We then outline the integration of this overlap reduction function in Sec. III and improve on the convergence of the resulting power series in Sec. IV. We present and discuss the results of numerical evaluations of the series in Sec. V. Finally, we conclude our formalism which we developed in the previous [1] and this paper in Sec. VI.

The detailed calculations were moved to Supplemental Material [9] to improve the readability of the main text.

## II. CORRELATIONS OF PTA SIGNALS

We cross-correlate two PTA signals which have been measured during the same time period and define their

mutual observation time as the length of the intersection of the time intervals  $I$  and  $I'$  in which the two pulsars  $a$  and  $a'$  have been observed:

$$T_{\text{obs}} := T(I \cap I'). \quad (1)$$

We will abbreviate  $T_{\text{obs}}$  to  $T$ .

The data  $d$  consist of the timing residuals  $r$  and the noise  $n$ ,

$$d(t) = r(t, \vec{\lambda}) + n(t), \quad (2)$$

where  $\vec{\lambda}$  is a parameter vector as, for example, the polarization modes  $\vec{\lambda} = (T, V, S)$  in the case of a gravitational wave background or the position of a source in the sky and the polarizations  $\vec{\lambda} = (\theta, \phi, +, \times, x, y, b, l)$  in the case of point sources.

To use matched filtering, we multiply a filter  $Q$  to the correlation:

$$Y := \int_0^T d(t) d'(t') Q(t - t') dt' dt. \quad (3)$$

The cross-correlated signal is the expectation of the filtered correlation and only depends on the two residuals, since the noise  $n_a$  is uncorrelated:

$$\mu := \mathbb{E}[Y] = \int_0^T \mathbb{E}[r(t, \vec{\lambda}) r'(t', \vec{\lambda}')] Q(t - t') dt' dt. \quad (4)$$

The variance of cross-correlated signals is given by [10]

$$\sigma^2 := \mathbb{V}[Y]|_{h=0} = \int_0^T \mathbb{E}[d(t) d(t') d'(\tau) d'(\tau')] Q(t - \tau) Q(t' - \tau') d\tau d\tau' dt = \frac{T}{4} \int P(|f|) P'(|f|) |\tilde{Q}(f)|^2 df, \quad (5)$$

where  $P_a$  is the noise power spectrum of pulsar  $a$ .

### A. Gravitational wave background

The GWB can be described by the power spectrum

$$\begin{aligned} & \mathbb{E}[\tilde{h}_A^*(f, \hat{\Omega}) \tilde{h}_{A'}(f', \hat{\Omega}')] \\ &= \delta(f - f') \frac{1}{4\pi} \delta(\hat{\Omega} - \hat{\Omega}') \delta_{AA'} \frac{1}{2} S_h^{A'}(|f'|). \end{aligned} \quad (6)$$

To reexpress the correlated signal in terms of the power spectral density of the GWB, we first have to Fourier transform it:

$$\begin{aligned} \mu &= \int_0^T \mathbb{E}[r(t, \vec{\lambda}) r'(t', \vec{\lambda}')] \int \tilde{Q}(f) e^{-2\pi i f(t-t')} df dt' dt \\ &= \int \mathbb{E} \left[ \underbrace{\int_0^T r(t, \vec{\lambda}) e^{-2\pi i f t} dt}_{\tilde{r}^*(f)} \underbrace{\int_0^T r'(t', \vec{\lambda}') e^{2\pi i f t'} dt'}_{\tilde{r}'(f)} \right] \tilde{Q}(f) df. \end{aligned} \quad (7)$$

The residual is defined as the time integral of the measured redshift  $z$ ,

$$r(t) = \int_0^t z(\tau) d\tau; \quad (8)$$

therefore, its Fourier transform is given by

$$\begin{aligned} \tilde{r}(f) &= \int_0^T \underbrace{\int_0^t z(\tau) d\tau}_{r(t)} e^{2\pi i f t} dt \\ &= -\frac{1}{2\pi i} \int \frac{\tilde{z}(\nu)}{\nu} \int_0^T e^{-2\pi i(\nu-f)t} dt d\nu \\ &\quad + \frac{1}{2\pi i} \int \frac{\tilde{z}(\nu)}{\nu} d\nu \underbrace{\int_0^T e^{2\pi i f t} dt}_{\approx 0, fT \gg 1} \\ &= -\frac{1}{2\pi i} \int \frac{\tilde{z}(\nu)}{\nu} \delta_T(\nu - f) d\nu. \end{aligned} \quad (9)$$

As seen in the proof of  $\lim_{\omega \rightarrow \infty} \int_a^b f(x) e^{i\omega x} dx = 0$  in (B2), only the two slices at the boundaries contribute to the integral, since the function  $f(x) = 1$  is constant in this case. If  $fT \gg 2\pi$ , then the integrand cancels on the largest part of the integration domain, and thus the integral is small compared to  $T$ , whereas the first integral is of order  $T$  ( $\delta_T(0) = T$ ). Therefore, the contribution of the second integral can be neglected.

To use the power spectrum, we need to express  $\tilde{z}$  in terms of  $\tilde{h}$ . To simplify the calculation, we express the frequency in terms of the angular frequency of the gravitational waves,  $2\pi f = \omega$ ,

$$\begin{aligned} \tilde{z}(\omega) &= \int_{-\frac{T}{2}}^{\frac{T}{2}} z_P(t) e^{i\omega t} dt \\ &= \int_{-\frac{T}{2}}^{\frac{T}{2}} \left\{ \frac{F^A \Delta h_A(t)}{1+\gamma} - \frac{\omega T_a F^A \Delta \dot{h}_A(t)}{2(1+\gamma)} + \frac{\delta\theta(t)}{2\pi} \right\} e^{i\omega t} dt \\ &= F^A \int_{-\frac{T}{2}}^{\frac{T}{2}} \frac{h_A(t) - h_A(t - \frac{L}{c}[1+\gamma])}{1+\gamma} e^{i\omega t} dt \\ &\quad - \frac{\omega T_a F^A}{2} \int_{-\frac{T}{2}}^{\frac{T}{2}} \frac{\Delta \dot{h}_A(t)}{1+\gamma} e^{i\omega t} dt + \int_{-\frac{T}{2}}^{\frac{T}{2}} \frac{\delta\theta(t)}{2\pi} e^{i\omega t} dt. \end{aligned} \quad (10)$$

A gravitational plane wave can be described as

$$\begin{aligned} \mu &= \frac{1}{4\pi^2} \int \frac{1}{\nu\nu'} \mathbb{E}[\tilde{z}^*(\nu) \tilde{z}'(\nu')] \delta_T(\nu - f) \delta_T(\nu' - f) d\nu' d\nu \tilde{Q}(f) df \\ &= \frac{1}{4\pi^2} \sum_A \int \frac{1}{2\nu^2} S_h^A(\nu) \delta_T^2(\nu - f) \frac{1}{4\pi} \int_{\mathbb{S}^2} F^A(\hat{\Omega}) F'^A(\hat{\Omega}) \frac{1 - e^{2\pi i \nu \tau}}{1+\gamma} \frac{1 - e^{-2\pi i \nu' \tau}}{1+\gamma'} d\hat{\Omega} d\nu \tilde{Q}(f) df \\ &= \frac{T}{24\pi^2} \int \frac{1}{f^2} \left[ \sum_M S_h^M(f) \Gamma_M \right] \tilde{Q}(f) df, \end{aligned} \quad (14)$$

where the power spectrum of a polarization mode is defined as the sum of the power spectra of both polarizations of that mode,  $S_h^M := S_h^{M_1} + S_h^{M_2}$ , and the overlap reduction functions are given by

$$\begin{aligned} \Gamma_M &:= \beta \int_{\mathbb{S}} (F^{M_1}(\hat{\Omega}) F'^{M_1}(\hat{\Omega}) + F^{M_2}(\hat{\Omega}) F'^{M_2}(\hat{\Omega})) \\ &\quad \cdot \frac{1 - e^{i\frac{L\omega}{c}[1+\gamma]}}{1+\gamma} \frac{1 - e^{-i\frac{L\omega'}{c}[1+\gamma']}}{1+\gamma'} d\hat{\Omega}, \end{aligned} \quad (15)$$

where  $\beta = \frac{3}{4\pi}$  is a normalization factor, which we chose to adopt from Ref. [11] for ease of comparison.

The overlap reduction function for the tensor mode is also called Hellings and Downs curve. It is usually assumed that the exponential terms can be neglected. We will

$$h_A(t, \vec{x}) = \frac{1}{2\pi} \int \tilde{h}_A(\omega) e^{-i\omega(t - \frac{\hat{\Omega} \cdot \vec{x}}{c})} d\omega. \quad (11)$$

And as derived in the previous paper [1], the amplitude difference is given by

$$\begin{aligned} \Delta h_A(t) &= h_A(t) - h_A(t_a) \\ &= \frac{1}{2\pi} \int \tilde{h}_A(\omega) [1 - e^{i\omega\tau}] e^{-i\omega t} d\omega, \end{aligned} \quad (12)$$

where  $t_a = t - \tau$  is the time, retarded by the retardation time  $\tau = \frac{L}{c}[1 + \gamma]$ .

We calculate the Fourier transform of the redshift for the leading-order term:

$$\begin{aligned} \tilde{z}(\omega) &\approx F^A \int \tilde{h}_A(f') \frac{1 - e^{2\pi i f' \tau}}{1+\gamma} \underbrace{\int_{-\frac{T}{2}}^{\frac{T}{2}} e^{-2\pi i(f'-f)t} dt}_{\delta_T(f'-f)} df' \\ &\approx F^A \tilde{h}_A(\omega) \frac{1 - e^{i\omega\tau}}{1+\gamma}. \end{aligned} \quad (13)$$

Plugging this expression back into the correlation signal, we get

calculate this overlap reduction function up to first order in  $h$  and zeroth order in  $h\omega T_a$  in the next section (Sec. III):

$$\begin{aligned} \Gamma_T &= \beta \int_{\mathbb{S}} (F^+(\hat{\Omega}) F'^+(\hat{\Omega}) + F^\times(\hat{\Omega}) F'^\times(\hat{\Omega})) \\ &\quad \cdot \frac{1 - e^{i\frac{L\omega}{c}[1+\gamma]}}{1+\gamma} \frac{1 - e^{-i\frac{L\omega'}{c}[1+\gamma']}}{1+\gamma'} d\hat{\Omega}. \end{aligned} \quad (16)$$

To maximize the scalar product

$$(A|B) := \int \tilde{A}^*(f) \tilde{B}(f) P(f) P'(f) df, \quad (17)$$

we choose the filter function to be

$$\tilde{Q}(f) = \frac{\sum_M S_h^M(f) \Gamma^M}{f^2 P(f) P'(f)}. \quad (18)$$

Rewriting signal and variance in terms of the scalar product and filter function, we get

$$\mu = \frac{T}{8\pi^2} (Q|Q), \quad \sigma^2 = \frac{T}{4} (Q|Q). \quad (19)$$

So, the signal-to-noise ratio is given by

$$\text{SNR} = \frac{1}{4\pi^2} \sqrt{T(Q|Q)} = \frac{1}{4\pi^2} \sqrt{T \int \frac{|\sum_M S_h^M(f) \Gamma^M|^2}{f^4 P(f) P'(f)} df}. \quad (20)$$

For more information about the matched filtering technique, see Appendix A.

### III. OVERLAP REDUCTION FUNCTION

As derived in the previous section, the overlap reduction function for the tensor mode for PTAs using natural units  $c = 1$  is given by

$$\Gamma_T = \beta \sum_{A \in \{+, \times\}} \int_{\mathbb{S}^2} F^A(\hat{\Omega}) F'^A(\hat{\Omega}) \frac{1 - e^{iL\omega[1+\gamma]}}{1 + \gamma} \frac{1 - e^{-iL'\omega[1+\gamma']}}{1 + \gamma'} d\hat{\Omega}. \quad (21)$$

To calculate this integral, we use the residue theorem on the  $\varphi$ -integral:

$$\Gamma_T = \sum_{A \in \{+, \times\}} \int_0^{2\pi} \int_0^\pi F^A(\hat{\Omega}) F'^A(\hat{\Omega}) \Delta h(\hat{\Omega}) \Delta h'(\hat{\Omega}) \sin \theta d\theta d\varphi = \int_0^\pi \oint_{C_1} f(z) dz d\theta = 2\pi i \int_0^\pi \text{Res}[f(z), 0] d\theta, \quad (22)$$

$$f(z) = \frac{(F^A F'^A \Delta h \Delta h')(\theta, z)}{iz} \sin \theta, \quad \Delta h = \frac{1 - e^{iL\omega[1+\gamma]}}{1 + \gamma}, \quad z = e^{i\varphi}.$$

The poles from the denominators  $\gamma = -1$  and  $\gamma' = -1$  are canceled by the nominators. Thus, the only pole left is the one at zero. To find the residue, we write the Laurent series of  $f$  around zero and read out the  $a_{-1}$ -term:

$$f(z) = \sum_{n \in \mathbb{Z}} a_n z^n, \quad \text{Res}[f(z), 0] = a_{-1}. \quad (23)$$

We chose our reference frame such that the pulsar  $a$  is located at  $\hat{x} = (1, 0, 0)$  and the second pulsar  $a'$  at  $\hat{x}' = (\cos \phi, \sin \phi, 0)$ . Then, complexified pattern functions

form a “generalized” polynomial in  $z$ . We write the exponential terms as a power series and use the geometric series to calculate the Laurent series of the  $\frac{1}{1+\gamma}$ -terms. We collect the (generalized) polynomial part in  $P(z) := z \sum_{n=-4}^4 b_n z^n$ ;  $b_{-n} = \bar{b}_n$ .

The powers in  $P$  are going to shift our  $a_{-1}$  term up and down the remaining series, which is a series multiplication of the exponential series part  $E$  and the geometric series part  $G$ . The exponential part contains positive and negative powers of  $z$ ,

$$E(z) = \sum_{n=0}^{\infty} \frac{1}{n!} \left( \frac{i\omega}{2z} \sin \theta \right)^n \{ -e^{iL\omega} L^n (1 + z^2)^n - e^{-iL'\omega} (-L')^n (e^{i\phi} + e^{-i\phi} z^2)^n + e^{i(L-L')\omega} (L - L' e^{i\phi} + [L - L' e^{-i\phi}] z^2)^n \}, \quad (24)$$

while the geometric series part only has positive powers of  $z$ ,

$$G(z) = \sum_{n=0}^{\infty} \sum_{k=0}^n (-1)^n e^{-ik\phi} \left( \frac{2}{\sin \theta} + e^{-i\phi} z \right)^k \left( \frac{2}{\sin \theta} + z \right)^{n-k} z^n. \quad (25)$$

With these definitions, we can write  $f$  as

$$f(z) = -\frac{ie^{-i\phi}}{8 \sin \theta} P(z) (1 + E(z)) G(z), \quad (26)$$

use the Cauchy product to write  $f$  as a series of nested sums, and sort the powers of  $z$  to read out the coefficient  $a_{-1}$  to calculate the  $\varphi$ -integral,

$$\int_0^{2\pi} F^A(\hat{\Omega}) F'^A(\hat{\Omega}) \Delta h(\hat{\Omega}) \Delta h'(\hat{\Omega}) \sin \theta d\varphi = \oint_{C_1} f(z) dz = 2\pi i a_{-1}, \quad (27)$$

which results in a series of nested sums of Bessel functions with  $\sin \theta$  as arguments. We use the linearity of integration and the fact that the resulting series converges absolutely to pull the  $\theta$ -integration in to the innermost terms, which are powers of sines and cosines,

$$\int_0^\pi \cos^m(\theta) \sin^n(\theta) d\theta = \frac{(1 + (-1)^m) \Gamma(\frac{1+m}{2}) \Gamma(\frac{1+n}{2})}{2\Gamma(\frac{1}{2}(2+m+n))}, \quad (28)$$

for  $\Re(m)$ , and  $\Re(n) > -1$ .

We finally obtain an analytic expression for the overlap reduction function for the tensor mode in form of an absolutely convergent series of nested sums:

We finally obtain an analytic expression in form of a series of nested sums for the overlap reduction function without short wavelength approximation. This series is absolutely convergent, and thus the expression is well defined for all angles  $\phi \in [0, \pi]$  (for the proof, refer to Supplemental Material [9]),

$$\begin{aligned} \Gamma_T = & \frac{\pi}{3} (3 + \cos \phi) - \frac{\pi}{8} e^{i\phi} [(1 + e^{-2i\phi}) h_{0,0,3,0,0}^+(\phi) + 2i(1 + e^{-i\phi}) h_{0,0,2,0,1}^-(\phi) + h_{0,0,3,0,2}^-(\phi)] \\ & + \frac{\pi}{4} e^{-i\phi} \left( \sum_{j=0}^1 (-2i)^j \sum_{k=0}^j \sum_{m=0}^k \sum_{l=0}^{j-k} \left(\frac{i}{2}\right)^{m+l} \binom{k}{m} \binom{j-k}{l} e^{-i(k+m)\phi} \right. \\ & \cdot \left\{ -\frac{e^{-2i\phi}}{2} h_{j,m+l,3,0,6}^+(\phi) + (1 + e^{2i\phi}) f_{j,m+l}(\phi) + (1 + e^{-2i\phi}) (h_{j,m+l,-1,4,4}^+(\phi) - h_{j,m+l,-1,0,4}^+(\phi)) \right. \\ & \left. \left. - \cos(2\phi) (h_{j,m+l,-1,0,2}^+(\phi) + 6h_{j,m+l,-1,2,2}^+(\phi) + h_{j,m+l,-1,4,2}^+(\phi)) - 2h_{j,m+l,3,0,2}^+(\phi) \right\} \right. \\ & + \sum_{j=2}^\infty (-2i)^j \sum_{k=0}^j \sum_{m=0}^k \sum_{l=0}^{j-k} \left(\frac{i}{2}\right)^{m+l} \binom{k}{m} \binom{j-k}{l} e^{-i(k+m)\phi} \\ & \cdot \left\{ -\frac{1}{2} (e^{2i\phi} h_{j,m+l,3,0,-2}^+(\phi) + e^{-2i\phi} h_{j,m+l,3,0,6}^+(\phi)) + (1 + e^{2i\phi}) f_{j,m+l}(\phi) \right. \\ & + (e^{-2i\phi} + 1) (h_{j,m+l,-1,4,4}^+(\phi) - h_{j,m+l,-1,0,4}^+(\phi)) \\ & \left. \left. - \cos(2\phi) (h_{j,m+l,-1,0,2}^+(\phi) + 6h_{j,m+l,-1,2,2}^+(\phi) + h_{j,m+l,-1,4,2}^+(\phi)) - 2h_{j,m+l,3,0,2}^+(\phi) \right\} \right), \quad (29) \end{aligned}$$

where we used the following definitions:

$$\begin{aligned} h_{j,b,s,t,N}^\pm(\phi) &:= \int_0^\pi \sin^{-j+b+s} \theta \cos^t \theta g_{j+b+N}(\theta) d\theta \\ &= \Gamma\left(\frac{t+1}{2}\right) \Gamma\left(k + \frac{s+N+1}{2}\right) \left[ e^{i(L-L')\omega} \left(\frac{1}{2}(L - e^{\pm i\phi} L')\omega\right)^{j+b+N} \right. \\ &\quad \times {}_1\tilde{F}_2\left(b + \frac{s+N+1}{2}; j+b+N+1, b + \frac{s+t+N}{2} + 1; -(L^2 + L'^2 - 2LL' \cos \phi) \frac{\omega^2}{4}\right) \\ &\quad - e^{iL\omega} \left(\frac{L\omega}{2}\right)^{j+b+N} {}_1\tilde{F}_2\left(b + \frac{s+N+1}{2}; j+b+N+1, b + \frac{s+t+N}{2} + 1; -\left(\frac{L\omega}{2}\right)^2\right) \\ &\quad \left. - e^{i(\pm(j+b+N)\phi - L'\omega)} \left(-\frac{L'\omega}{2}\right)^{j+b+N} {}_1\tilde{F}_2\left(b + \frac{s+N+1}{2}; j+b+N+1, b + \frac{s+t+N}{2} + 1; -\left(\frac{L'\omega}{2}\right)^2\right) \right] \quad (30) \end{aligned}$$

and

$$\begin{aligned}
 f_{j,b}(\phi) &:= \int_0^\pi \sin^{-j+b-1} \theta (\cos^4 \theta - 1) g_{j+b}^+(\theta) d\theta \\
 &= \sqrt{\pi} 2^{-j-b} \Gamma(b+1) \Gamma(b+3) \left[ e^{iL\omega} (L\omega)^{j+b} {}_2\tilde{F}_3 \left( b+1, b+3; j+b+1, b+2, b+\frac{5}{2}; -\left(\frac{L\omega}{2}\right)^2 \right) \right. \\
 &\quad + e^{i((j+b)\phi - L'\omega)} (-L'\omega)^{j+b} {}_2\tilde{F}_3 \left( b+1, b+3; j+b+1, b+2, b+\frac{5}{2}; -\left(\frac{L'\omega}{2}\right)^2 \right) \\
 &\quad \left. - e^{i(L-L')\omega} ((L - e^{i\phi} L')\omega)^{j+b} {}_2\tilde{F}_3 \left( b+1, b+3; j+b+1, b+2, b+\frac{5}{2}; -(L^2 + L'^2 - 2LL' \cos \phi) \frac{\omega^2}{4} \right) \right]. \quad (31)
 \end{aligned}$$

#### IV. OPTIMIZATION OF THE OVERLAP REDUCTION FUNCTION

If we evaluate (29) and add the terms in that sequence, we would not add the largest terms first, and thus in this way, the numerical convergence is computationally inefficient, since one would add a lot of small and potentially irrelevant terms, before one adds the next larger term.

Since the series is absolutely convergent, which we show in the Supplemental Material [9], we can reorder the series such that the largest terms are added first. This also allowed us to simplify some terms and in doing so get rid of two sums. With that, we arrive at the final expression,

$$\begin{aligned}
 \Gamma_T &= \frac{\pi}{3} (3 + \cos \phi) - \frac{\pi}{8} e^{i\phi} [(1 + e^{-2i\phi}) h_{0,0,3,0,0}^+(\phi) + 2i(1 + e^{-i\phi}) h_{0,0,2,0,1}^-(\phi) + h_{0,0,3,0,2}^-(\phi)] \\
 &\quad + \frac{\pi}{4} e^{-i\phi} \left( \sum_{j=0}^1 (-2i)^j \sum_{k=0}^j \sum_{m=0}^k \sum_{l=0}^{j-k} \left(\frac{i}{2}\right)^{m+l} \binom{k}{m} \binom{j-k}{l} e^{-i(k+m)\phi} \right. \\
 &\quad \cdot \left\{ -\frac{e^{-2i\phi}}{2} h_{j,m+l,3,0,6}^+(\phi) + (1 + e^{2i\phi}) f_{j,m+l}(\phi) + (1 + e^{-2i\phi}) (h_{j,m+l,-1,4,4}^+(\phi) - h_{j,m+l,-1,0,4}^+(\phi)) \right. \\
 &\quad \left. \left. - \cos(2\phi) (h_{j,m+l,-1,0,2}^+(\phi) + 6h_{j,m+l,-1,2,2}^+(\phi) + h_{j,m+l,-1,4,2}^+(\phi)) - 2h_{j,m+l,3,0,2}^+(\phi) \right\} \right. \\
 &\quad + \sum_{a=2}^{\infty} (-2i)^a \sum_{b=0}^{\lfloor \frac{a}{2} \rfloor} \left(-\frac{1}{4}\right)^b \left\{ -\frac{1}{2} (e^{2i\phi} h_{a,b,3,0,-2}^+(\phi) + e^{-2i\phi} h_{a,b,3,0,6}^+(\phi)) + (1 + e^{2i\phi}) f_{a,b}(\phi) \right. \\
 &\quad + (e^{-2i\phi} + 1) (h_{a,b,-1,4,4}^+(\phi) - h_{a,b,-1,0,4}^+(\phi)) - \cos(2\phi) (h_{a,b,-1,0,2}^+(\phi) + 6h_{a,b,-1,2,2}^+(\phi) + h_{a,b,-1,4,2}^+(\phi)) \\
 &\quad \left. - 2h_{a,b,3,0,2}^+(\phi) \right\} \sum_{k=0}^{a-b} \left\{ \begin{aligned} &e^{-ik\phi} \binom{a-b-k}{b} {}_2F_1(-b, -k; 1+a-2b-k; e^{-i\phi}) & a \geq 2b+k \\ &e^{i(a-2(b+k))\phi} \binom{k}{a-2b} {}_2F_1(-a+2b, -a+b+k; 1-a+2b+k; e^{-i\phi}) & a < 2b+k \end{aligned} \right\}, \quad (32)
 \end{aligned}$$

where  $h_{a,b,s,t,N}^\pm(\phi)$  and  $f_{a,b}(\phi)$  were redefined by using the substitution

$$j, k, m, l \rightarrow a = j + m + l, \quad b = m + l, k, m. \quad (33)$$

#### V. DISCUSSION OF THE RESULTS

We assure ourselves that the numerical evaluation of the truncated series (sum until a suitable cutoff) agrees with a straightforward numerical integration via the trapezoidal rule and compare the analytic series to the approximation obtained by Hellings and Downs.

To investigate the dependence on  $L\omega$ , we compare the results for different values of  $L\omega$  for the special case  $L = L'$ , where the two correlated pulsars are at the same distance and for large distance ratios  $\frac{L}{L'}$ .

Some representative results are plotted in Fig. 1. The imaginary part always vanishes in the case where  $L = L'$  since the only complex part of the integrand is phase differences  $(1 - e^{iL\omega[1+\gamma_a]})(1 - e^{-iL'\omega[1+\gamma_{a'}]})$  and in this special case they become complex conjugates of each other and thus the integrand is real. It is not a surprise then that we observe bigger imaginary parts for larger distance ratios  $\frac{L}{L'}$ . It might sound a bit strange that an



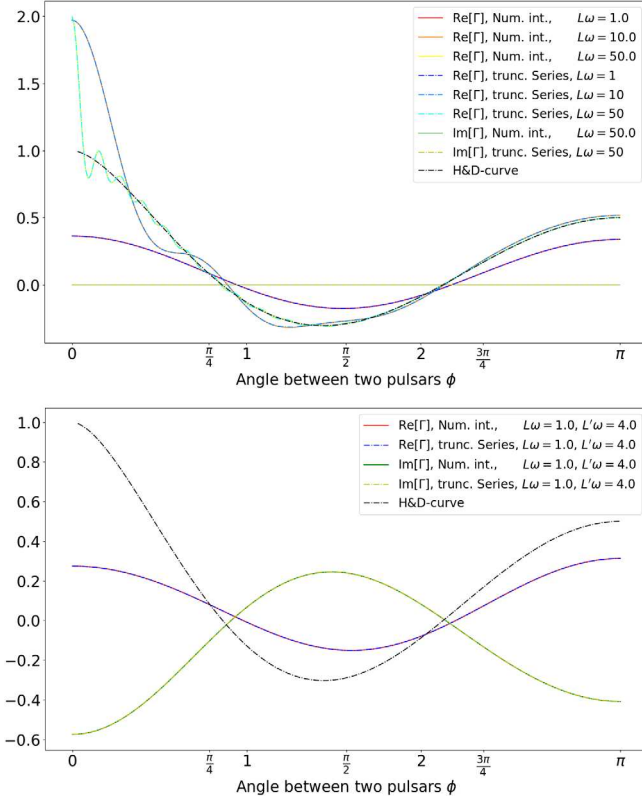


FIG. 1. A comparison between numerical integration and evaluation of the truncated analytical series for different values of  $L\omega$  and  $L'\omega$ , in the cases where  $L = L'$  (upper) and  $L \neq L'$  (lower). The solid lines show the numerical integrations, the dot-dashed lines show the truncated series, and the black dashed line is the Hellings and Downs curve.

overlap reduction function is complex, but it appears in the SNR only with its absolute value, and thus this physical quantity remains real.

We investigate the limit of large  $L\omega$  in the case  $L = L'$  by plotting the truncated series from  $L\omega = 1$  up to  $L\omega = 100$ , where a evaluation on a laptop is still feasible. After that, the numerical evaluation of the three nested sums becomes very expensive even for a single point. Since the inner sums are dependent on the outer ones, further parallelization is a nontrivial task, which we chose to not engage in. It can already be seen from Fig. 2 that the problematic region around  $\phi = 0$  becomes smaller for larger  $L\omega$  and that the value at  $\phi = 0$  converges to 2, contrary to the limit of  $\phi \rightarrow 0$  obtained from the H&D curve. We also observe that the function always oscillates in the region  $[0, \frac{\pi}{2}]$ . A deviation from the signal by  $\pm 3\%$  would still give good result when doing matched filtering. This behavior becomes even more obvious in Fig. 3.

We conclude that for large  $L\omega$  in the case where both pulsars are at the same distance from Earth  $L = L'$  the series converges to the H&D curve everywhere except of  $\phi = 0$  where it converges to 2.

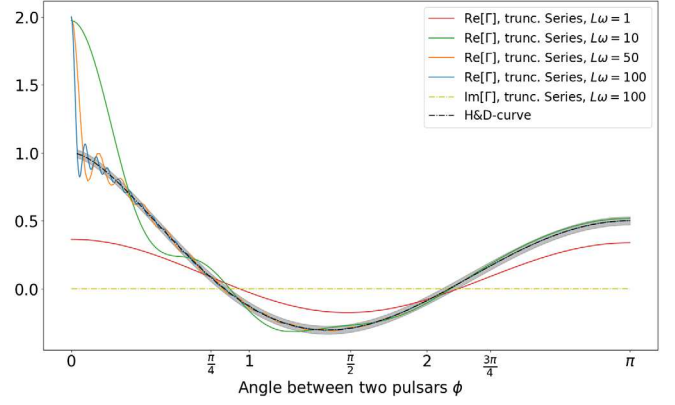


FIG. 2. We plot the truncated series for  $L\omega$  over 3 orders of magnitude in the special case of  $L = L'$ , to empirically investigate the convergence for large  $L\omega$ . We compare our results to the Hellings and Downs curve (black dashed line). The area in gray marks the 3% deviation from the H&D curve, which is unproblematic for matched filtering.

Now that we know what happens at different orders of magnitudes of  $L\omega$  for equal distances, we are interested in how different pulsar distances affect the result. We observe in Fig. 4 that the correlation at  $\phi = 0$  decays from 2 to 1 over a difference of only 5% in  $L\omega$ , which then agrees with

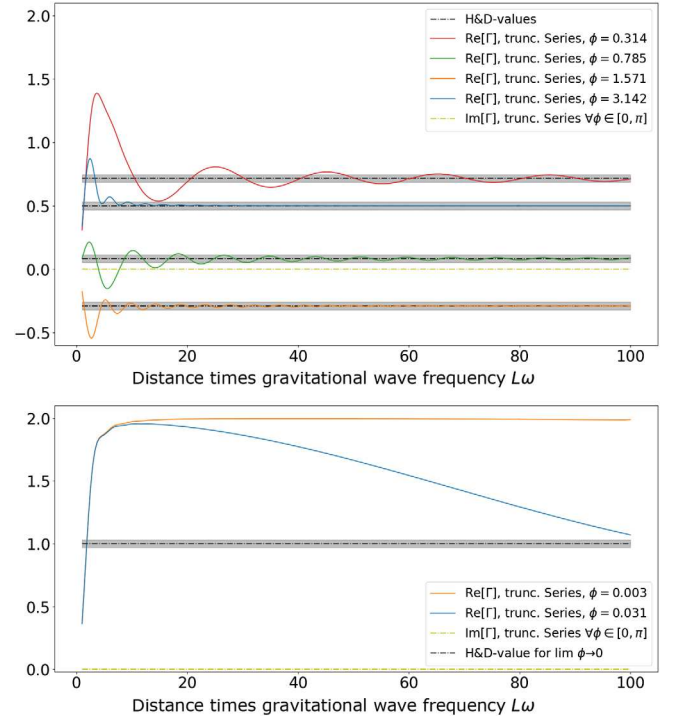


FIG. 3. In the plot above, we sample the parameter space for the separation angle  $\phi$  and plot the overlap reduction function as a function of distance times gravitational wave frequency  $L\omega$  in the case of  $L = L'$ . Below, we show the same plot for  $\phi$ -values close to zero. We compare the two curves to the limit of the H&D curve for  $\phi$  tending to zero.



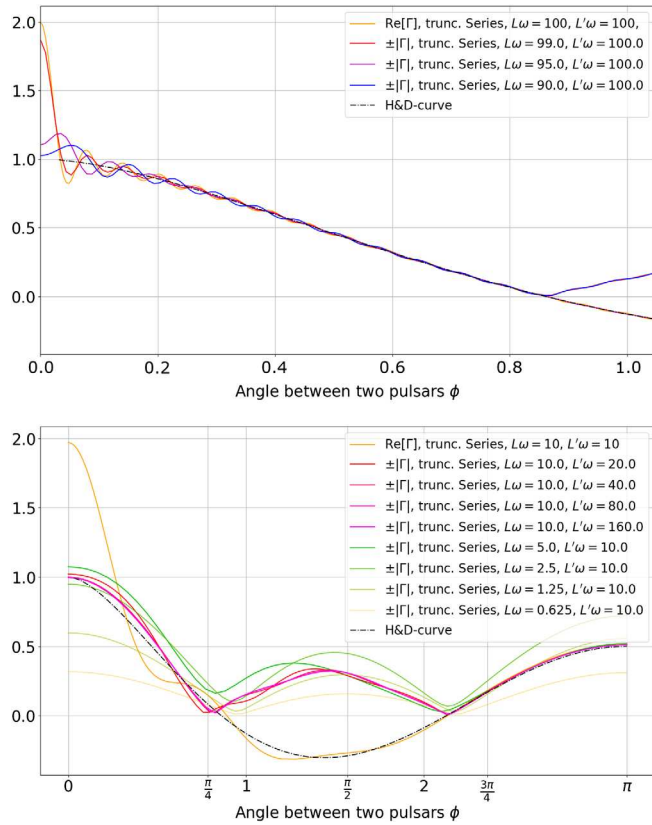


FIG. 4. We plot the series for small differences in the pulsar distance  $\frac{L'}{L} \approx 1$  around  $L\omega = 100$  in the upper panel and for large ratios in the lower panel. There, we use  $L\omega = 10$  as a reference value. The curves where  $L'\omega$  is below 10 are the purple ones, and the ones where  $L'\omega$  is bigger than 10 are red. We plot the special case  $L = L'$  in orange and the H&D curve in dashed black for comparison.

the limit obtained from H&D, and that it converges more quickly to the H&D curve than when  $L = L'$ . This means that it is only realistic to have a factor of 2 for a double pulsar system. The complex overlap reduction functions do not always cross zero. In the cases in which they do, we change the sign in front of the absolute value for a better comparison with the H&D curve. Since only the absolute value is relevant for the SNR, the sign choices are inconsequential.

From the plots above Figs. 1, 2 and 4, 5, we see that for higher  $L\omega$  the peak at  $\phi = 0$  and  $L = L'$  becomes narrower and the neighborhood around this point where the short wavelength approximation does not apply becomes smaller. This is due to the pulsar term becoming relevant in this part of the parameter space. Thus, we expect that for all current observationally relevant  $L\omega$  our result agrees with the Hellings and Downs curve, with the only exception being double pulsar systems for, e.g., Ref. [6]. Despite the fact that the overlap reduction function depends on the pulsar distances, one does not require precise distance measurements in this frequency regime. We either have a

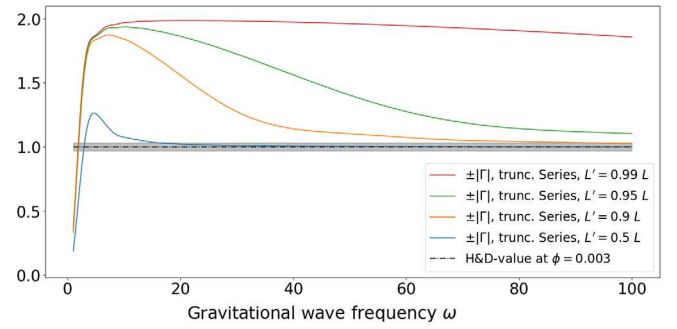


FIG. 5. We plot the gravitational wave frequency  $\omega$  dependence of the overlap reduction function, focusing on distance ratios close to 1, at the separation angle  $\phi = \frac{\pi}{1000}$ .

double pulsar system, in which the pulsars orbit each other and they are for all intents and purposes colocated; i.e., both the angular separation and difference in distance are negligible and there is a much larger redshift due to the pulsar orbits. In this case, the overlap reduction function would assume the value 2. Or the pulsar systems do not form a double pulsar system and are separated by much larger distances, such that they do not affect each others orbit. In this case, for  $L\omega$  around 1000 or higher, the function would assume the value 1 *due* to rapid decay of the peak at such high  $L\omega$  values.

## VI. CONCLUSIONS

Together with our previous paper [1], we developed a methodology to calculate the redshift and overlap reduction functions, which is generally applicable for all polarizations and pulsar locations. We expect it to work also for higher-order terms in the strain  $h$  and gravitational wave frequency times pulsar period  $\omega T_a$  and even without any approximation in  $\omega T_a$ . We gave a semianalytical form of the redshift for a generic gravitational wave with all possible (including non GR) polarizations without expansion in  $\omega T_a$  and a power series for the overlap reduction function to first order in  $h$  and zeroth order in  $\omega T_a$  for the tensor mode. (This can be extrapolated to other polarization modes.)

The approximation which was used by Ref. [8] and described as noise by Ref. [11] is the one we derive in Appendix B. We find that this is only justified under the condition (B6) which cannot be satisfied at  $\phi = 0$  where the integrand has a pole but works fine on  $\phi \in [\epsilon, 2\pi]$  for a large enough  $\epsilon$  dependent on the required precision and parameter  $L\omega$  one is interested in. The Hellings and Downs curve

$$\Gamma_0 = 3 \left\{ \frac{1}{3} + \frac{1 - \cos \phi}{2} \left[ \ln \frac{1 - \cos \phi}{2} - \frac{1}{6} \right] \right\},$$

$$\lim_{\phi \rightarrow 0} \Gamma_0 = 1 \quad (34)$$

is not well defined at  $\phi = 0$  since the argument of the logarithm goes to zero. The limit of  $\phi \rightarrow 0$  exists, however, but disagrees with the exact result, which is always 2 at that point since the two signals in the correlation optimally stack up. It is basically putting two detectors on top of each other and thus gaining twice the signal since the only difference in the two measurements is their independent noise. If the distances  $L$  and  $L'$  to the two pulsars are not the same, however, the two signals differ more with increasing  $\Delta L = |L - L'|$ , and thus the correlation decays, and  $\Gamma_T$  tends to 1.

It turns out that as  $L\omega$  increases the absolute values of the first summands in the series become larger and larger. In fact, their absolute values lie orders of magnitudes above the value of the final result, which is between 0 and 2. And even though the peak goes farther away from the start  $a = 2$ , the first terms cannot be neglected since they are always of order 1 and the way larger terms will cancel precisely until the result becomes of order 1. So, the most successful method has been to find out at which *index*  $a$  the terms become smaller than  $10^{-5}$  and sum until there, and then one only has to add a handful of additional terms until one cannot see the curve change anymore (additional term was less than or approximately equal to  $10^{-3}$  everywhere). Thus, the variable *aStart* in the code can actually be deleted; it always has to be 5 anyways.

Because of the canceling in extreme cases from  $10^{90}$  down to 1, the precision was a big issue. We used *Mathematica* [12] for this reason to do the numerical calculations since we could just choose higher initial precisions to make sure that at the end of the calculation enough meaningful digits were left.

Another surprise was that for larger  $\phi$  one had to choose larger cutoffs, although the function very quickly converged to the Hellings and Downs curve and was not oscillating as strong as for  $\phi$  around zero.

It should be noted that the formalism and the results presented in this paper do not change the value of the overlap reduction function obtained using H&D for most of the pulsar systems currently used for gravitational wave searches with PTA. Our formalism changes the value of the overlap reduction function only for a subpopulation of colocated pulsars which can be used for gravitational wave searches. These systems can be potentially rare as the pulsars used for gravitational wave searches are traditionally millisecond pulsars. Pulsars in double-neutron-star binaries are unlikely to get fully recycled and hence will not be fast spinning with

sufficiently low spindown rates [13]. However, in the future with SKA, one will discover a huge population of pulsars with chances of finding rare systems. If a suitable double-neutron-star binary is discovered, it would be the most sensitive system for gravitational wave searches, and hence applying the formalism presented in this paper would be necessary to make use of them.

## ACKNOWLEDGMENTS

We thank the anonymous referee for suggesting numerous improvements to the paper, especially for suggesting the inclusion of Fig. 5. A. B. is supported by the Forschungskredit of the University of Zurich Grant No. FK-20-083 and by the Tomalla Foundation. S. T. is supported by Swiss National Science Foundation Grant No. 200020 182047.

## APPENDIX A: MATCHED FILTERING

The idea is that if one multiplies the signal  $h$  to the strain  $s = h + n$  in the integral then the signal is squared and thus positive on the entire domain, while the signal times the noise  $nh$  can have both signs, and since they are not correlated, this contribution becomes small,

$$\int_U s(t)h(t)dt = \int_U h^2(t) + n(t)h(t)dt \approx \int_U h^2(t)dt, \quad (\text{A1})$$

where we integrate over the domain  $U \subset \mathbb{R}$ .

To use this effect, we multiply our cross-correlated strain from detectors  $a$  and  $b$  with a filter function  $Q$ . The goal will then be to find the best possible filter function to do this. Since we want to overlay signals that arrived at different times at the two detectors and thus get rid of the choice of  $t_0 = 0$ , we chose the filter to depend on the time difference:

$$Y := \int s(t)s'(t')Q(t-t')dt'dt. \quad (\text{A2})$$

However, now our expression  $Y$  is dependent on the filter function, which we choose, and does not represent the correlated signal anymore. To get rid of this dependence, we have to divide it out. Therefore, we take the signal-to-noise ratio and expand it with  $Q$  by multiplying it into the integrals of the nominator and denominator:

$$\text{SNR} = \frac{\mu}{\sigma} = \frac{\int h(t)h'(t')dt'dt}{\sqrt{\int n(t)n(t')n'(\tau)n'(\tau')d\tau d\tau' dt}} \quad (\text{A3})$$

$$\mapsto \text{SNR}[Q] = \frac{\int s(t)s'(t')Q(t-t')dt'dt}{\sqrt{\int n(t)n(t')n'(\tau)n'(\tau')Q(t-\tau)Q(t'-\tau')d\tau d\tau' dt}}. \quad (\text{A4})$$

This is not a strict expansion of the fraction, however, and the effect of the filter function does not divide out, which will allow us to maximize the SNR by choosing an appropriate filter.

To maximize the SNR with the filter function, we define a scalar product and reexpress the signal-to-noise ratio in terms of the scalar product:

$$(A|B) := \int \tilde{A}^*(f) \tilde{B}(f) P(f) P'(f) df$$

$$\rightarrow \mu[Q] = \left( \frac{hh'}{PP'} \middle| Q \right), \quad \sigma[Q] = \sqrt{\frac{T}{4} (Q|Q)}. \quad (\text{A5})$$

The SNR is maximal if the scalar product  $\mu[Q]$  is maximal, and thus the optimal filter function  $Q_{\text{opt}}$  has to be chosen parallel to  $\frac{hh'}{PP'}$ .

With this choice, the filtered signal can be rewritten in terms of the optimal filter function, and the best signal-to-noise ratio one can achieve this way is given by

$$\text{SNR}[Q_{\text{opt}}] = \frac{\mu[Q_{\text{opt}}]}{\sigma[Q_{\text{opt}}]} = \frac{(Q_{\text{opt}}|Q_{\text{opt}})}{\sqrt{\frac{T}{4} (Q_{\text{opt}}|Q_{\text{opt}})}} = 2\sqrt{\frac{(Q_{\text{opt}}|Q_{\text{opt}})}{T}}. \quad (\text{A6})$$

To get to the signal we get by using matched filtering, we cannot just plug  $Q_{\text{opt}}$  into  $\mu[Q]$  since this expression does not represent the signal due to its dependency on  $Q$ . The SNR, however, does represent the signal-to-noise ratio we get by using this method because we divide the filter function out. So, what we can do to get to our signal is multiply the SNR with the noise that remains after matched filtering.

To get an expression for our filter independent noise, we use the same trick as above and expand the noise with  $Q$ ,

$$\sigma^2 = \mathbb{V}[\mu] \mapsto \sigma_{\text{MF}}^2 = \frac{\mathbb{V}[\mu[Q]]}{\int Q^2 dt}, \quad (\text{A7})$$

where  $\sigma_{\text{MF}}$  denotes the remaining noise after the signal has been filtered with  $Q$ .

We can again express everything in terms of the scalar product, for  $Q = Q_{\text{opt}}$ :

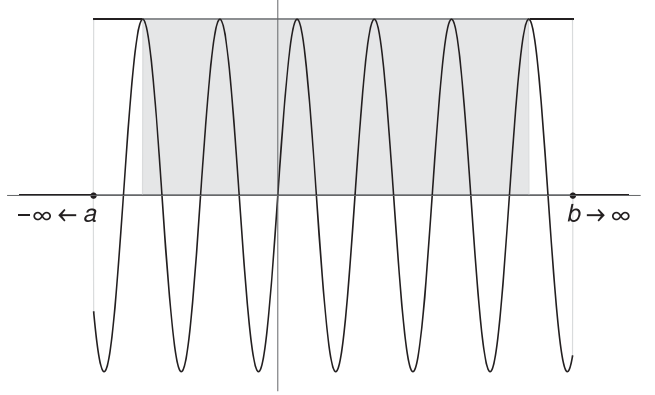


FIG. 6. The part of the function, which lies in the grey area does not contribute to the integral, since its oscillations cancel. Only a segment on each side contributes, which is always smaller than one period.

$$\mathbb{V}[Q_{\text{opt}}] = \frac{T}{4} (Q_{\text{opt}}|Q_{\text{opt}}), \quad \int |Q_{\text{opt}}(f)|^2 df = \frac{(Q_{\text{opt}}|Q_{\text{opt}})}{P(f_0)P'(f_0)}$$

$$\Rightarrow \sigma_{\text{MF}}^2 = \frac{T}{4} P(f_0)P'(f_0). \quad (\text{A8})$$

We now finally get an expression for the matched filtered signal:

$$\mu_{\text{MF}} = \text{SNR}[Q_{\text{opt}}] \cdot \sigma_{\text{MF}} = \sqrt{(Q_{\text{opt}}|Q_{\text{opt}})P(f_0)P'(f_0)}. \quad (\text{A9})$$

## APPENDIX B: SHORT WAVELENGTH APPROXIMATION

In many cases in physics, rapidly oscillating terms are being neglected (short wavelength approximation) and considered as small with respect to other terms in the integral if the frequency is very high. This comes from the fact that a constant function times  $e^{i\omega x}$  is arbitrarily small compared to the integral over the constant function as one lets the integration domain become infinite. The idea is sketched in Fig. 6,

$$\lim_{a \rightarrow -\infty} \lim_{b \rightarrow \infty} \frac{1}{b-a} \int_a^b e^{i\omega x} dx \leq \lim_{a \rightarrow -\infty} \lim_{b \rightarrow \infty} \frac{1}{b-a} \left( \int_a^{a+\frac{2\pi}{\omega}} |e^{i\omega x}| dx + \int_{b-\frac{2\pi}{\omega}}^b |e^{i\omega x}| dx \right) = 0. \quad (\text{B1})$$

We give a proof that in the following case, which is essentially the limit for  $\omega \rightarrow \infty$  of an inverse Fourier transform restricted on the interval  $[a, b] \subset \mathbb{R}$ , this holds:

$$\lim_{\omega \rightarrow \infty} \int_a^b f(x) e^{i\omega x} dx = 0, \quad \text{if } f'(x) < \infty \quad \forall x \in [a, b]. \quad (\text{B2})$$

*Proof.*—Let  $\varepsilon = \frac{2\pi}{\omega}$ ,  $N = \lfloor \frac{b-a}{\varepsilon} \rfloor$ ,  $x_n = a + n\varepsilon$ , and  $f'_m = \max\{f'(x) | x \in [a, b]\}$ .

In the limit of  $\varepsilon \rightarrow 0$ , the approximation of a smooth function  $f$  with a piecewise linear one becomes precise. We do this on intervals which comprise exactly one period of the oscillation. At the end, there will be a small piece of the domain left due to rounding with a length smaller than  $\varepsilon$ :

$$\lim_{\omega \rightarrow \infty} \int_a^b f(x) e^{i\omega x} dx = \lim_{\varepsilon \rightarrow 0} \left\{ \sum_{n=0}^{N-1} \int_0^\varepsilon (f'(x_n)x + f(x)) e^{i\omega x} dx + \int_{a+N\varepsilon}^b f(x) e^{i\omega x} dx \right\}. \quad (\text{B3})$$

The first integral can be solved by partial integration:

$$\begin{aligned} \left| \lim_{\varepsilon \rightarrow 0} \sum_{n=0}^{N-1} \int_0^\varepsilon (f'(x_n)x + f(x)) e^{i\omega x} dx \right| &= \left| \lim_{\varepsilon \rightarrow 0} \sum_{n=0}^{N-1} f'(x_n) \left[ e^{i\omega \varepsilon} \left( \frac{1}{\omega^2} - \frac{i\varepsilon}{\omega} \right) - \frac{1}{\omega^2} \right] + \lim_{\varepsilon \rightarrow 0} \sum_{n=0}^{N-1} \frac{f(x_n)}{i\omega} [e^{i\omega \varepsilon} - 1] \right| \\ &\stackrel{\omega \varepsilon = 2\pi}{=} \left| \frac{1}{2\pi i} \sum_{n=0}^{N-1} f'(x_n) \varepsilon^2 \right| \leq \frac{b-a}{2\pi} \lim_{\varepsilon \rightarrow 0} |f'_m| \varepsilon = 0. \end{aligned} \quad (\text{B4})$$

Since the second integral is only over a fraction of the domain, smaller than  $\varepsilon$ , we can construct an upper bound:

$$\begin{aligned} \lim_{\varepsilon \rightarrow 0} \left| \int_{a+N\varepsilon}^b f(x) e^{i\omega x} dx \right| \lim_{\varepsilon \rightarrow 0} &\leq \varepsilon |\max\{f(x) | x \in [b-\varepsilon, b]\}| \\ &= \lim_{\varepsilon \rightarrow 0} \varepsilon f(b) = 0. \end{aligned} \quad (\text{B5})$$

One could use  $\frac{b-a}{2\pi} |f'_m| \varepsilon + \varepsilon |f(b)|$  as an error estimate for large but finite  $\omega$ . It is not proven to be a strict upper bound, however, since we approximated the function with a piecewise linear function and we did not give an upper bound for this error in the finite case.

In the case of the overlap reduction function for PTA's, the exponential term is of the form  $e^{i\omega g(x)}$ , and thus we have to generalize the result above to use it:

$$\lim_{\omega \rightarrow \infty} \int_a^b f(x) e^{i\omega g(x)} dx = 0, \quad \text{if } \frac{f'g' - fg''}{(g')^3} < \infty \quad \forall x \in [a, b]. \quad (\text{B6})$$

*Proof.*—

$$\lim_{\omega \rightarrow \infty} \int_a^b f(x) e^{i\omega g(x)} dx = \lim_{\omega \rightarrow \infty} \int_{g(a)}^{g(b)} \frac{f}{g'}(g^{-1}(y)) e^{i\omega y} dy. \quad (\text{B7})$$

With the substitution  $y = g(x)$ ,  $dy = g'(x)dx$ , we brought the integral into the simpler form and can now apply the result from above:

$$\begin{aligned} \left| \lim_{\omega \rightarrow \infty} \int_{g(a)}^{g(b)} \frac{f}{g'}(g^{-1}(y)) e^{i\omega y} dy \right| &\leq \frac{|g(b) - g(a)|}{2\pi} \lim_{\varepsilon \rightarrow 0} \max_y \left\{ \frac{d}{dy} \left( \frac{f}{g'} \circ g^{-1} \right)(y) \right\} \varepsilon \\ &= \frac{|g(b) - g(a)|}{2\pi} \lim_{\varepsilon \rightarrow 0} \max_x \left\{ \frac{d}{dx} \left( \frac{f}{g'} \right)(x) \frac{dy}{dx} \right\} \varepsilon = \frac{|g(b) - g(a)|}{2\pi} \lim_{\varepsilon \rightarrow 0} \max_x \left\{ \frac{f'g' - fg''}{(g')^3}(x) \right\} \varepsilon = 0. \end{aligned} \quad (\text{B8})$$

- [1] A. Boîtier, S. Tiwari, L. Philippoz, and P. Jetzer, *Phys. Rev. D* **102**, 064051 (2020).
- [2] S. J. Chamberlin and X. Siemens, *Phys. Rev. D* **85**, 082001 (2012).
- [3] G. Hobbs *et al.*, *Classical Quantum Gravity* **27**, 084013 (2010).
- [4] B. Perera *et al.*, *Mon. Not. R. Astron. Soc.* **490**, 4666 (2019).
- [5] R. N. Manchester *et al.*, *Pub. Astron. Soc. Aust.* **30**, e017 (2013).
- [6] A. G. Lyne, M. Burgay, M. Kramer, A. Possenti, R. N. Manchester, F. Camilo, M. A. McLaughlin, D. R. Lorimer, N. D'Amico, B. C. Joshi, J. Reynolds, and P. C. C. Freire, *Science* **303**, 1153 (2004).
- [7] B. J. Owen, *Phys. Rev. D* **53**, 6749 (1996).
- [8] R. W. Hellings and G. S. Downs, *Astrophys. J.* **265**, L39 (1983).
- [9] See Supplemental Material at <http://link.aps.org/supplemental/10.1103/PhysRevD.103.064044> for all the detailed calculations outlined in sections III and IV, which have been mentioned via Ref. [9] in these sections. They describe, how we arrange the two dimensional integral into two nested one dimensional ones, where we calculate the inner one by calculating the residue via reading out the  $-1$ -th Laurent series coefficient and then the outer one using the main theorem of calculus. We then reorder the series, which we got as a result of this process, as outlined in the main text. In the appendix we deal with some special integrals and terms which occur in the calculation and prove the absolute convergence of the series to make sure, that reordering it does not change its limit.
- [10] L. Philippoz, A. Boîtier, and P. Jetzer, *Phys. Rev. D* **98**, 044025 (2018).
- [11] M. Anholm, S. Ballmer, J. D. E. Creighton, L. R. Price, and X. Siemens, *Phys. Rev. D* **79**, 084030 (2009).
- [12] W. R. Inc, *Mathematica*, Ver. 12.1, Champaign, IL, 2019.
- [13] D. Bhattacharya and E. P. J. van den Heuvel, *Phys. Rep.* **203**, 1 (1991).